ce/papers Proceedings in civil engineering

Ernst & Sohn A Wiley Brand

ORIGINAL ARTICLE

ibausil F. A. Finger-Institut für Baustoffkunde Bauhaus-Universität Weimar

# Fracture behavior of ultra-high performance light-weight concrete: In situ investigations using µ-CT

Cristin Umbach[1] | Bernhard Middendorf[1]

**Correspondence**

Cristin Umbach
University of Kassel
Inst. for Structural Engineering
Dept. of Structural Materials and Construction Chemistry
Mönchebergstraße 7
34125 Kassel
Email: c.umbach@uni-kassel.de

[1] University of Kassel, Kassel, Germany

**Abstract**

In various research projects at the University of Kassel, the concept of lightweight concrete has been combined with that of ultra-high performance concrete (UHPC). Due to the high performance of the UHPC matrix, lightweight concretes (UHPLC) with strengths of 60-130 MPa and bulk density of 1.5-1.9 kg/m³ were developed. This material can be used in many applications because of its low thermal conductivity, low weight and thus easy to transport, recyclable and can be prefabricated. Thus, it meets today's multifunctional requirements for building materials. The brittle material failure of UHPC without fibers is not observed with UHPLC. Instead, the concretes fail in hourglass shape under compressive stress, as seen in standard concretes. This constellation is not only responsible for the reduction of strength and Y-modulus, but also predicts a ductile failure. For a better interpretation of the fracture behavior and fracture pattern, images of the UHPLC were taken in a high-resolution computed tomography (µ-CT) scanner. Between images, the sample was loaded and the load was kept constant during the measurement. The data was evaluated on the basis of a damage parameter, as well as crack openings during stable crack growth and the crack pattern after the maximum load was exceeded.

**Keywords**

Lightweight concrete, in situ µ-CT, fracture behavior, ultra-high performance concrete

## 1 Introduction

High-strength concrete (HPC) and ultra-high-strength concrete (UHPC) offer the possibility of building more filigree and thus lighter structures [1]. UHPC is characterized by a compressive strength of > 150 MPa and a very dense microstructure [2]. The properties of UHPC have been extensively investigated in research programs. One of the most extensive research programs was funded by the German Research Foundation (DFG) under the priority program SPP 1182, the results are summarized in [1]. The development of the material investigated in the following work is based on the fine-grained UHPC mix M3Q used in this program. This UHPC is a very well studied material whose durability is guaranteed by its structural density.

Structural lightweight concretes are a combination of a dense cement paste matrix and lightweight aggregates [3]. Due to the lightweight aggregate, the load transfer through the porous structures is disturbed and consequently reduced. Furthermore, the type of a lightweight aggregate influences the properties of the fresh and hardened concrete. An industrially produced aggregate is expanded glass which was used in this work. This lightweight aggregate is also available in very fine particle sizes, but its compressive strength of 2.8 N/mm² (particle size 0.1-0.3 mm) is comparatively low. However, expanded glass has the advantage that it has a closed sintered skin and therefore absorbs less water than open porous aggregates.

Thus, the building material considered in the following is a structural lightweight concrete with expanded glass, which is produced with a UHPC matrix in order to obtain a high-performance, lightweight building material with low thermal conductivity and low weight. This means that this material can be used in a wide range of applications because, in addition to the advantages mentioned above, it is easy to transport, recyclable and can be prefabricated. Thus, it meets today's multifunctional requirements for building materials. However, the influence of the lightweight aggregates in UHPC on the mechanical properties is hitherto not well understood because it is a new class of material, ultra-high performance lightweight concrete (UHPLC). The fracture behavior of UHPLC is of particular interest because it ensures the stability of structures. Brittle, abrupt failure of building materials is undesirable because no action can be taken to secure the structure in case of unannounced failure. Since UHPC fails brittle, preventive measures such as the addition of steel fibers, must be used to maintain a



https://doi.org/10.1002/cepa.2852

ductile fracture pattern and residual capacity.

The fracture behavior of lightweight concrete is described by the final fracture pattern according to the theory of Grübel [4]. Different load paths and thus different fracture patterns are explained for different matrix strengths. Another theory by Faust [5] assumes that the proportion and strength of the lightweight aggregate is essential for the performance.

To better understand and interpret the fracture behavior and the resulting fracture pattern, images of UHPLC with expanded glass were obtained using high-resolution computed tomography (µ-CT) while the specimens were subjected to in situ compressive loading. 3D images were generated at five different loading conditions without unloading the specimens in between.

## 2 Materials and methods

### 2.1 Ultra-high performance lightweight concrete

To produce a UHPLC, the cement paste matrix of M3Q [1] was combined with expanded glass to reduce the density. In order to optimize the packing density, suitable raw materials have to be selected. In addition to cement and aggregate, these include fillers such as stone powder and reactive components such as silica fume. The results from the characterization of these starting materials can be used to calculate the optimum packing.

To produce different density classes of lightweight concretes with the expanded glass, the quartz sand was volumetrically partially or completely substituted by different expanded glass (EG) fractions. The grains were selected to achieve a high packing density and the density classes D1.6, D1.8, and D2.0 (Table 1).

The mixes were prepared using an Eirich R05T intensive mixer with a nominal volume of 40 L. The homogenized dry materials were intensively mixed for two minutes together with water, superplasticizer and mass hydrophobizer. Mixing was then repeated at low energy for another five minutes. Five minutes after the end of mixing, the slump flow test and the $t_{500}$ time were determined according to German Standard EN 12350-8 [6]. The tests were performed in an air-conditioned room at 20 °C and 65 % RH. All three concretes can be classified in slump flow class SF 2 according to German Standard EN 206 [3]. According to the standard, the concrete is therefore suitable for many common applications such as walls and columns.

All prepared specimens were taken out of the mold after 24 hours and stored at 20°C and 65% RH until testing. The specimens for the µ-CT studies were drilled from cubes with an edge length of 15 cm after 7 days using a core drilling machine. The core dimensions were 8 mm in diameter and approximately 20-50 mm in length. Samples of 8 mm in length were cut from these cores another seven days later using a precision cutter (Buehler; IsoMet Low Speed). Earlier processing time was not possible because the cores would be broken. Since the specimens had a height difference of about 0.1 mm due to inaccuracies in drilling and sawing, they were levelled with a mixture of Portland cement (Holcim Sulfo 5R), alumina cement (Imerys Aluminates; Ciment Fondu), and quartz powder (Quarzwerke; W3). For adjusting, the thinnest possible layer of cement paste was applied to both sides of the specimens. This resulted in a total height of approximately 8.1 mm.

**Table 1** Mix design of UHPLC with different bulk density classes and UHPC [1]

| raw material | unit | EG D1.6 | EG D1.8 | EG D2.0 | UHPC [1] |
|---|---|---|---|---|---|
| **cement Holcim Sulfo 5R** | kg/m³ | | 771.90 | | 775.00 |
| **silica fume Sika Sillicoll P uncompacted** | kg/m³ | | 163.65 | | 164.00 |
| **superplasticizer Sika ViscoCrete 2810** | % bwoc.[1)] | | 3.9 | | 3.0 |
| **hydrophobing agent Sika Control AE-10** | % bwoc.[1)] | | 2.0 | | - |
| **quartz flour Quarzwerke Millisil W12** | kg/m³ | | 199.00 | | 193.00 |
| **quartz sand Quarzwerke G32** | kg/m³ | - | 338.99 | 627.76 | 946.00 |
| **expanded glass Poraver 0.1-0.3 mm** | kg/m³ | - | 49.86 | 29.43 | - |
| **expanded glass Poraver 0.25-0.5 mm** | kg/m³ | 122.45 | 128.83 | 67.61 | - |
| **expanded glass Poraver 0.5-1 mm** | kg/m³ | 94.75 | - | - | - |
| parameters of mix design | | | | | |
| **water/binder ratio** | kg/kg | | 0.21 | | |
| **dry bulk density** | kg/m³ | 1.51 | 1.72 | 1.90 | 2.30 |

1) by weight of cement

## 2.2 Mechanical tests

Compressive strength was determined on three cubes of 100 mm edge length according to German Standard EN 12390-3 [7] (Figure 1). All tests were force-controlled with a test rate of 0.5 N/mm²s. After 7 days, the strength was plotted against the bulk density at climatic storage (20°C, 65% RH). After 28 days, the strengths are plotted against dry bulk density (oven dried to mass consistency).

In principle, it can be seen that the strength increases with increasing bulk density. This can be observed for all lightweight concretes [8] and is due to the decreasing porosity. Mixture EG D1.6 reaches an average final strength of 63.2 MPa after 7 days at a bulk density of 1,510 kg/m³. This mix contains only expanded glass in two grain sizes as aggregate, while the other two mixes contain quartz sand in addition to expanded glass.

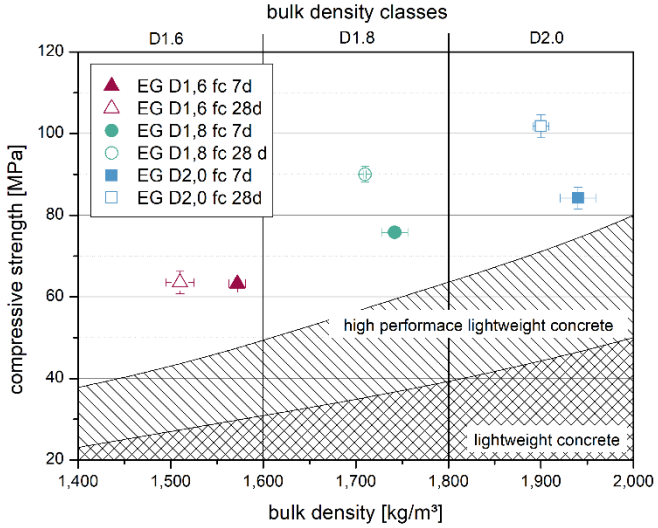


**Figure 1** Compressive strength of EG D1.6, EG D1.8 and EG D2.0 mixes as a function of dry bulk density. Classification of strength ranges for lightweight and high strength lightweight concrete according to [8]

The Young's modulus was determined according to German Standard EN 12390-13 [9] on cylinders with a diameter of 100 mm and a height of 200 mm (Fig. 2). The test was performed using method B.

For normal concrete, the modulus of elasticity $E_{cm}$ depends on the compressive strength (see German Standard EN 1992-1-1 [10], Table 3.1). For lightweight concrete, there is an additional dependence on the bulk density ρ. Therefore, according to EN 1992-1-1 [10], Tab. 11.3.1, the modulus of elasticity $E_{lcm}$ can be reduced by the factor $\eta_E$ in comparison to normal concrete according to equation (1):

$$E_{lcm} = \eta_E E_{cm} \text{ mit } \eta_E = \left(\frac{\rho}{2200}\right)^2 \quad (1)$$

In general, the measured Young's modulus increases with increasing bulk density, in this case by about 5 GPa per bulk density class. Without the influence of bulk density, all three concretes had approximately the same stiffness.

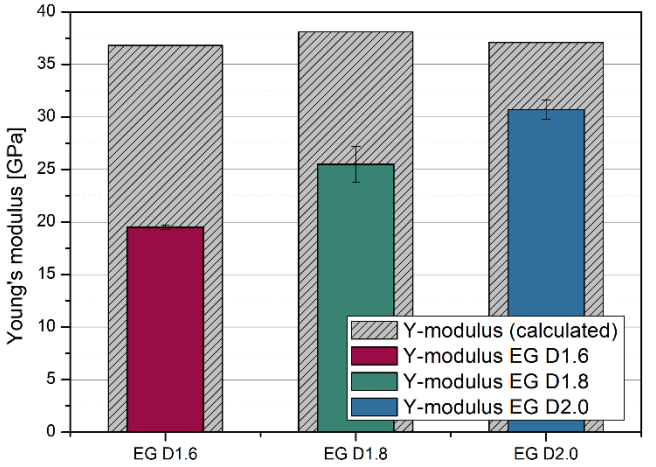


**Figure 2** Young's modulus of EG D1.6, EG D1.8 and EG D2.0 mixes as a function of dry bulk density

## 2.3 High-resolution computed tomography

Computed tomography can be used to show differences in density in a three-dimensional image. The basic function of computed tomography is to reconstruct an object from its projections. The object is irradiated with x-rays at different angles and the projection is recorded on a detector (Figure 3). In the images, denser areas are light and less dense areas are dark. Therefore, the air appears black in the images, while the cement paste and aggregate appear in various gray values.

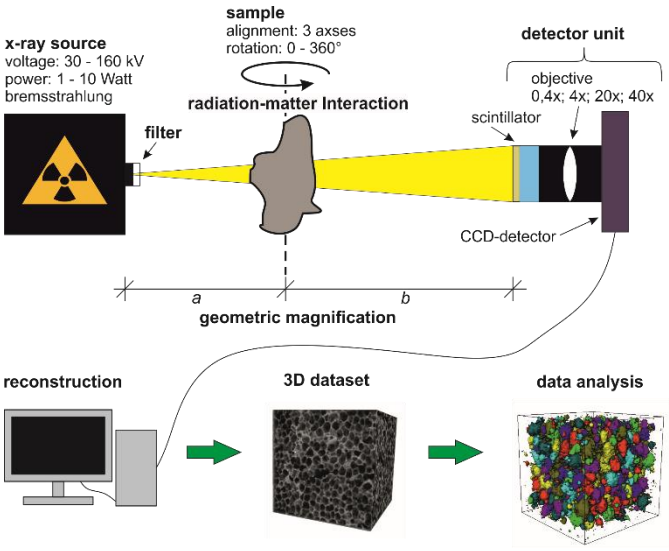


**Figure 3** Scheme of the functional principle of a µ-CT with parameters of the Xradia 520 Versa device [11]

The measurement method of high-resolution computed tomography (µ-CT) is defined by a resolution in the one- to two-digit µm range, which can be achieved by using objectives (X-ray microscope). The instrument used, the Xradia 520 Versa from Zeiss Microscopy, has a spatial resolution of 0.7 - 50 µm. In order to visualise cracks in material samples in three dimensions, high resolutions in the range of a few micrometres are required. This is influenced by several factors of the physical measuring principle. The choice of settings is therefore important to the success of the measurement. The basic settings of the µ-CT are listed in Table 2.

**Table 2** General measurement settings of the used µ-CT

| unit | part | setting |
|---|---|---|
| **source** | voltage/ power | 140kV/ 10W |
| | acquisition time | 10 sec |
| **detector** | type | objective 4x + CCD |
| | binning | 2 |
| **scan** | acquisition area | 5,120 µm x 5,120 µm |
| | resolution | 5.0 µm |
| **recon-struction** | type | filtered back projection |

### 2.4 In situ testing

In the in situ method, concrete specimens are progressively loaded between measurements so that crack growth within the specimen is visible. The advantages of in situ loading are:

- measurement without intermediate unloading
- the same area is always measured
- crack growth can be observed between measurements.

Figure 4 shows the Microtest CT5000RT load frame used in µ-CT. The position of the specimen and the load are also shown schematically.

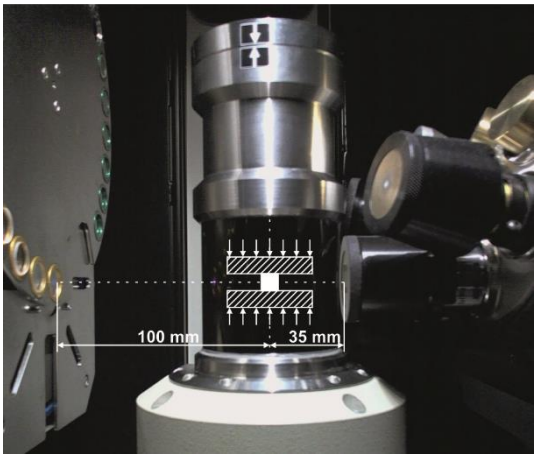


**Figure 4** Sample positioning in the µ-CT with Microtest CT5000RT load frame

A total of 5 images were taken from one specimen under different load conditions:

1. unloaded
2. at 30% of maximum load
3. at 90% of maximum load
4. at 100% of load
5. after failure.

Five specimens were used to determine the maximum load for programming the load frame. These were prepared in the same way as the other specimens and loaded in the load frame without interruption and µ-CT measurement.

Based on the boundary conditions resulting from the technical conditions of the load frame on the one hand and the required resolution of the µ-CT measurement on the other hand, a drill core with a diameter of 8 mm was selected as sample geometry. The specimen was measured slightly eccentrically in order to make the crack development visible at the edge and in the center.

### 2.5 Evaluation of 3D datasets

The analysis of the 3D datasets was performed with the program Avizo 9.5. The general procedure for the analysis is:

1. determination of the "region of interest" (ROI)
2. filtering
3. segmentation
4. mathematical analysis of the segmented objects
5. evaluation.

#### 2.5.1 Region of Interest

The data sets were trimmed at the edges for analysis. This was done to avoid the influence of different physical and reconstruction artifacts which occur at the edges of a measurement.

#### 2.5.2 Filtering

Filtering datasets is used to highlight or emphasize certain features of the structures. This is done by transforming the image and outputting the desired information or improving the appearance of the data [12].

For this purpose, the nonlinear nonlocal means (NLM) filter was used. This filter is characterized by its ability to preserve contours while effectively suppressing noise. Figure 5 shows a sectional view of a filtered image.

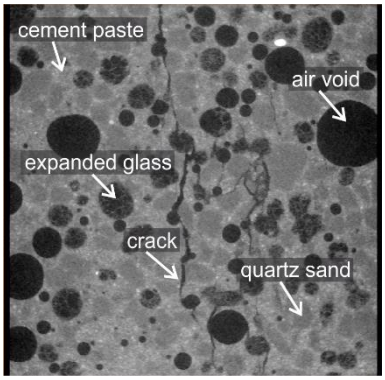


**Figure 5** Overview of a filtered µ-CT image with an image width of 5 mm

#### 2.5.3 Segmentation

Segmentation is the most error-prone step, since setting a threshold affects whether a pixel/voxel belongs to one region or another (binarization). For this reason, automated methods exist in addition to manual methods. For this work, an automated thresholding method, Otsu Thresholding [13], was chosen. The segmentation should differentiate between porosity (air voids and entrapped air in expanded glass grains) and dense material (cement

paste and quartz sand).

From the binary data set, the individual objects are considered one at a time (labelling). A representation with different colors for different objects is shown in Figure 6. For the 5 measurements, the overall condition is shown on one side and the crack on the other.

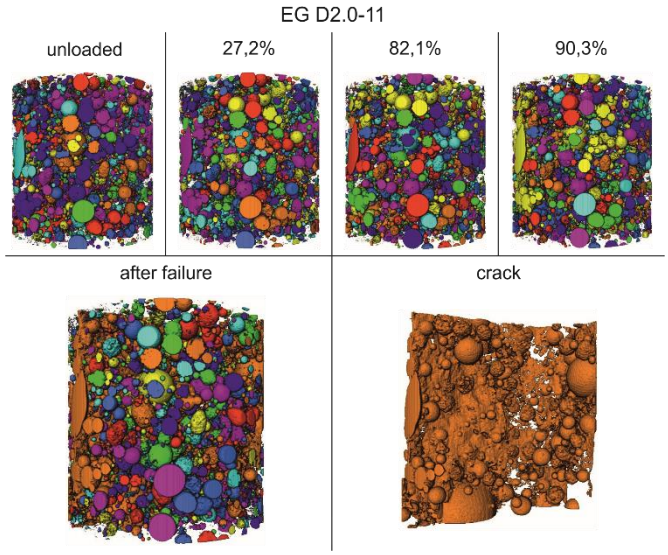


**Figure 6** Model of air inclusions in specimen EG D2.0-11 after different loading conditions. Cylinder diameter 5 mm

### 2.5.4 Mathematical Analysis

There are many ways to evaluate the segmented and gray value data. Only the information used is described below.

Histograms of gray values can be derived from reconstructions. The frequency of occurrence of a voxel of a given color is plotted from 0 (black) to 65,535 (white). To compare the histograms of a series of measurements, they were plotted as a line graph.

The volume is determined by counting the number of voxels that make up an object. Thus, the volume V of an object is a multiple of the volume of a voxel $V_i$. From this, porosity P can be determined (2) using the total volume $V_{tot}$.

$$P\,[\%] = \frac{100}{V_{tot}} \sum V_i \qquad (2)$$

The damage due to crack volume change indicates how the volume of porosity changes, since in addition to air, cracks and microdefects also represent porosity. To obtain the damage parameter, the volume of porosity $V_D$ was divided by the total volume $V_{tot}$. This generated a unit less value that will take the value of 1 when the porosity is 100% (3).

$$\omega_V = \frac{V_D}{V_{tot}} \qquad (3)$$

To obtain the damage as a difference value, the first value, which represented the starting porosity, was subtracted from the other values.

## 3 Evaluation

The specimens from the EG D2.0 test series showed the most significant results, as cracks were also found here that did not directly lead to failure of the entire specimen, and thus belonged to stable crack growth. Therefore, these specimens are shown in the figures 7-9.

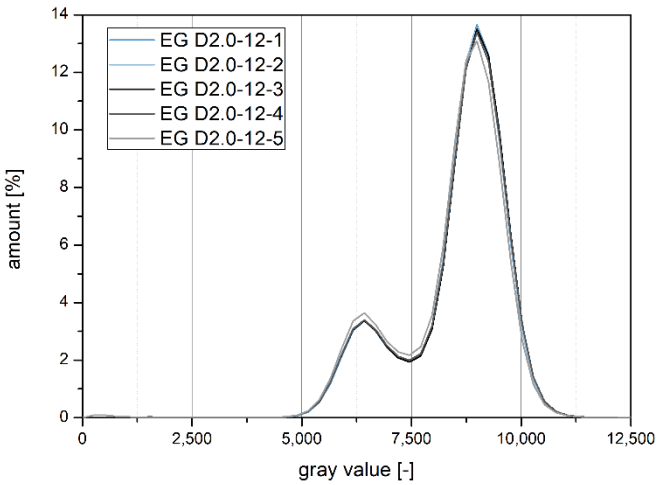


**Figure 7** Histograms of the measurement EG D2.0-12 at the measurement points 1-5

In general, two peaks can be seen in the plotted histograms. The first peak represents the porosity and the second represents the hardened cement paste matrix. As an example, figure 7 shows the histograms of sample EG D2.0-12. The last number in the label indicates the load condition of measurement (cf. chapter 2.4). A closer look reveals a shift to darker colors towards the end of the measurement series.

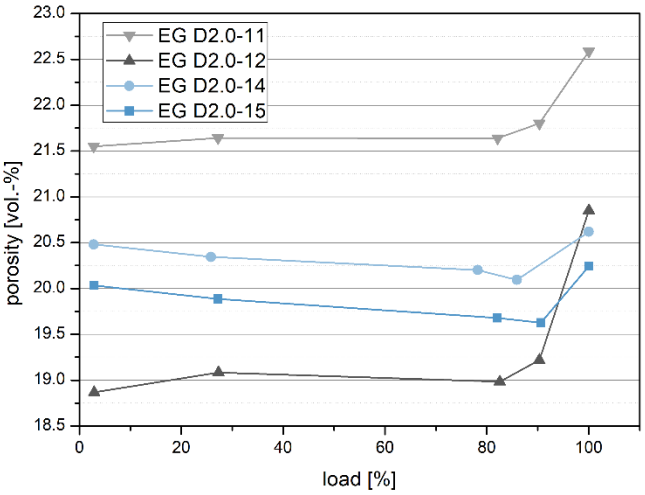


**Figure 8** Porosity in the specimens of the EG D2.0 test series during loading

All measurements in a series were segmented with the same threshold. Figure 8 shows the volume fraction of that segmentation plotted against load. It can be seen that in the images of specimens EG D2.0-13 and -14, the porosity decreases until the last measurement and increases only in the last measurement, where the crack occurs. In these images, no cracks were found in the microstructure at almost 90% of the load.

In contrast, an increase in porosity was observed in the fourth scan of the scan series of specimens -11 and -12.

In these scans, cracks were found in the microstructure. Since only a partial area of the specimens was recorded, it cannot be excluded that specimens -13 and -14 also had cracks in the microstructure at the 90% load.

The calculation of the damage parameter resulting from the observed damage volume shows that even a small defect fraction of 0.002 – 0.02 is sufficient to lead to a failure of the entire sample (Figure 9). Considering all measurement series, a maximum damage parameter $\omega_V$ of 0.04 was determined.

Negative values are also shown in the graph. These are the result of microstructural consolidation and represent an improvement in the structure in terms of porosity. It can be seen that the specimens that cracked at about 90% load did not show any densification of the microstructure. This difference in load bearing behavior could not be correlated with compressive strength. The strength was constant with a variation of 0.97 MPa.

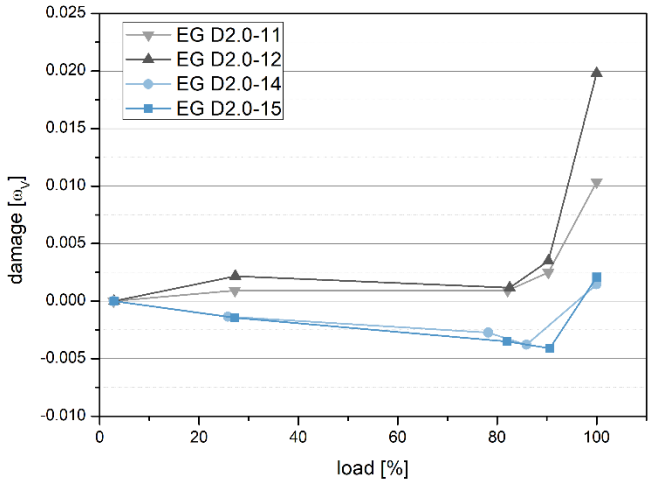


**Figure 9** Damage parameter due to crack volume change for specimen EG D2.0 test series during loading

For many specimens, the fracture pattern can only be seen in the final state because no cracks or defective structures were recorded in the last image before failure. Defective structures would be, for example, broken expanded glass, which fails like described in [4]. However, the specimens either withstood the load without damage or failed because the load was too close to the failure limit. The cracks that opened were unstable, resulting in a drop in stress. The load frame, which was supposed to hold the set stress, tried to rebuild the stress by closing the load plates, which was not possible because the cracks kept opening. This process was stopped either manually or by controlling the minimum opening width of the load frame.

The specimens where stable crack growth was observed show that the cracks opened vertically in the specimen, i.e., orthogonal to the load application, and had start or end points in air voids or expanded glass (Figure 10). In addition, as is more commonly observed in UHPC, the crack propagated through quartz grains (red arrow) as well as at the interface (green arrow). The corresponding 3D model of the crack also showed the extensive branching. The red frame indicates the location of the 2D section in the 3D model. After the fracture, and thus the failure of the matrix, a second crack was visible in many places next to the first crack (yellow arrow). This was further from the crack opening than the first crack observed in this part of the specimen. This indicates that tensile forces were diverted into the surrounding material and the force became higher than the tensile strength of the material at this new location. This then led to the ultimate failure of the specimen.

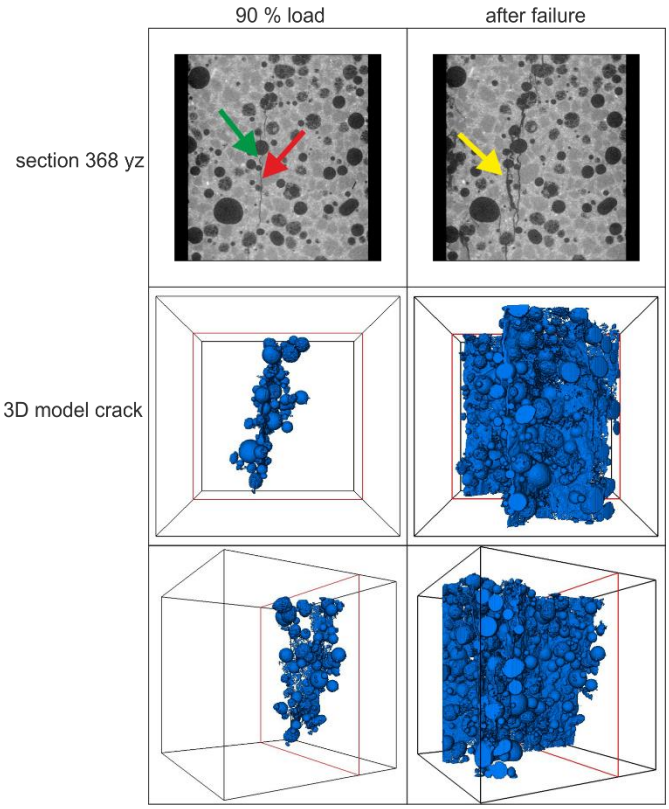


**Figure 10** Fracture pattern of specimen EG D2.0 -12 at 90% of the maximum load and after failure. The red frame shows the position of the 2D section in the 3D model (edge length 5 mm)

## 4 Conclusion

Lightweight concretes are becoming more and more important in prefabricated wall elements because of their high thermal insulation and low weight. With regard to sustainable building, UHPLC will certainly be increasingly used in the future due to its multifunctional capability. According to Grübel [4], a concrete with a light aggregate and a cement paste matrix strength of > 90 N/mm² fails by so-called grain fracture. In this case, the grains break and no longer participate in the load transfer, which ultimately leads to the failure of the entire system. Since this is a process that takes place inside the concrete, a CT measurement is one of the few ways to study the behavior of the concrete in situ under load. In almost all specimens, a compaction of the microstructure was observed first, which was released by the formation of cracks or when the specimen failed. The following observations were made:

- no grain fracture according to [4]
- cracks between lightweight aggregates or air voids in the UHPC matrix
- compaction of the microstructure under load
- crack opening in the ITZ or sintered skin of the expanded glass
- the final fracture pattern shows fractured expanded glass grains.

The fracture pattern of all the lightweight concretes tested was hourglass shaped. Thus, the overall picture is the same as for normal concrete, i.e., at the limit of lateral restraint, the tensile forces are exceeded and the specimens crack. In this case, the crack follows the path of least stiffness, which in lightweight concrete is dictated by the lightweight aggregate and air voids.

In the present work, the internal structure of lightweight concrete under load could be observed for the first time. This is only possible by using a µ-CT. Due to the large density difference between air and material, cracks could be observed even before the maximum load was applied. The in situ loading allowed the specimens to be examined without intermediate unloading, allowing the microstructure to be evaluated under elastic deformation. The results of the work have provided a unique insight into the fracture behavior of lightweight concretes, but can also be applied to other concrete systems.

**Acknowledgement**

The results presented in this paper are part of a dissertation. The dissertation was submitted at University of Kassel in March 2023. Publication is pending at the submission date of this paper.

**References**

[1] Schmidt M. et al. (2014*) Sustainable Building with Ultra-High Performance Concrete – Results of the German Priority Programme 1182 funded by Deutsche Forschungsgemeinschaft (DFG)*. Kassel: kassel university press.

[2] Schmidt M. et al. (2008) *Sachstandsbericht Ultrahochfester Beton*, Berlin: Ernst & Sohn Verlag.

[3] EN 206:2013+A2:2021. *Concrete—Specification, Performance, Production and Conformity*; European Committee for Standardization, Berlin, Germany, 2021.

[4] Grübl P. (1979) *Druckfestigkeit von Leichtbeton mit geschlossenem Gefüge*, Beton, vol. 1979 no. 3, pp. 91-95.

[5] Faust T. (2003): *Leichtbeton im Konstruktiven Ingenieurbau.* Berlin: Ernst & Sohn Verlag.

[6] EN 12350-8:2008*. Testing fresh concrete- Part 8: Self-compacting concrete –Slump-flow test;* European Committee for Standardization: Beuth Verlag, Berlin, Germany, 2008.

[7] EN 12390-3:2019. *Testing Hardened Concrete—Part 3: Compressive Strength of Test Specimens*; European Committee for Standardization: Beuth Verlag, Berlin, Germany, 2019.

[8] Thienel K.-C. (1996) *Materialtechnologische Eigenschaften der Leichtbetone aus Blähton*.In: TFB Seminar: Leichtbetone im konstruktiven Ingenieurbau, Wildegg, Schweiz.

[9] EN 12390-13:2015. *Testing Hardened Concrete—Part 13: Determination of secant modulus of elasticity in compression*. European Committee for Standardization: Beuth Verlag, Berlin, Germany, 2015.

[10] EN 1992-1-1:2011. *Eurocode 2: Design of concrete structures – Part 1-1: General rules and rules for buildings*. European Committee for Standardization: Beuth Verlag, Berlin, Germany, 2019.

[11] Umbach C., Middendorf B. (2019) *3D structural analysis of construction materials using high-resolution computed tomography*. Materials Today: Proceedings, vol. 15, pp. 356-363.

[12] Burger W., Burge M. J. (2015) *Digitale Bildverarbeitung*. Berlin & Heidelberg: *Springer Verlag*.

[13] Otsu N. (1979) *A Threshold Selection Method from Gray-Level Histograms*. In: *IEEE Transactions on Systems, Man, and Cybernetics*, vol. 9 no. 1, pp. 62-66.